Hindawi
Advances in Civil Engineering
Volume 2021, Article ID 6688746, 20 pages
https://doi.org/10.1155/2021/6688746

Research Article

Field Measurement and Numerical Simulation of Train-Induced Vibration from a Metro Tunnel in Soft Deposits

Qiang Huang,[1,2] Pan Li ,[2,3] Dongming Zhang,[2,3] Hongwei Huang,[2,3] and Feng Zhang[4]

[1]*School of Civil and Environmental Engineering, Ningbo University, Ningbo 315211, China*
[2]*Key Laboratory of Geotechnical and Underground Engineering of the Ministry of Education, Tongji University, Shanghai 200092, China*
[3]*Department of Geotechnical Engineering, Tongji University, Shanghai 200092, China*
[4]*Department of Geotechnical Engineering, Nagoya Institute of Technology, Nagoya 466-8555, Japan*

Correspondence should be addressed to Pan Li; yongpanli@163.com

Received 21 October 2020; Revised 24 December 2020; Accepted 19 January 2021; Published 16 February 2021

Academic Editor: Weerachart Tangchirapat

Train-induced vibration is increasingly attracting people's concern nowadays. In the coastal areas, many metro tunnels are built in the soft deposits, so the train-induced vibration effect is more serious. Nevertheless, the existing research studies mainly focus on the dynamic responses in the tunnel or on the ground surface while vibration characteristics in the ground are seldom studied. In this paper, a comprehensive field measurement was performed by installing accelerometers in the tunnel and soil layers and on the ground surface to capture the response characteristics of the track-tunnel-ground system. Elastoplastic numerical simulation considering the soil-water coupling was conducted to reveal the responses of acceleration, dynamic displacement, and excess pore water pressure using FE code DBLEAVES. Measurement results indicate that high-frequency contents (>500 Hz) attenuate rapidly in the propagation process; the dominant frequency of the rail concentrates in the middle- and high-frequency bands, about 25–400 Hz and 1000–1500 Hz, while the frequencies of the track bed, soil layers, and ground surface drop to below 400, 200, and 100 Hz, respectively. The vertical ground acceleration decreases like an arc in the transverse direction while there is transverse acceleration amplification phenomenon at a distance from the upper haunch and lower haunch of the tunnel. Overall, the area affected by train vibration in the soft deposits is about 30 m away from the metro tunnel. Numerical simulation based on soil-water coupled analysis is feasible to model the vibration characteristics in the soft deposits and confirms that there is acceleration amplification in the ground. Moreover, numerical results indicate that excess pore water pressure can be accumulated during each train vibration, so the train-induced settlement will be a potential problem in the long term for the metro tunnel.

1. Introduction

Nowadays, urban rail transit is rapidly developed to alleviate the increasing transportation pressure. Although urban rail transit greatly facilitates the transportation of the public, it also generates environmental vibration problem in return. The train-induced vibration causes discomfort to residents and disturbance to sensitive equipment in buildings near the tunnel; the vibration sometimes reaches a level that can hardly be tolerated by the residents in adjacent buildings [1, 2]. As the number of the railway lines continues to increase, the train-induced vibration has become an issue of great concern. For example, the European Union launched a program called CONVURT to investigate the ground-borne vibration characteristics of the underground tunnels [3].

In some coastal areas, such as Shanghai of China, metro tunnels are mostly built in the soft deposits, typical lacustrine or marine soil layers, with low strength, high compressibility, and high sensitivity, and the mechanical properties are so poor that the train-induced vibration effect is more serious. For instance, the soft ground can be disturbed by the train vibration load and produces plastic deformation and excess pore water pressure, which may induce dynamic settlement to the metro tunnels in the long term [4,5]. Hence, the train-induced vibration from a metro tunnel in the soft deposits should be carefully considered in

particular. Generally speaking, there are analytical approach, field measurement, and numerical calculation methods in dealing with the train-induced vibration. For example, some researchers have obtained the 2D and 3D analytical solutions of the coupled tunnel-ground system [6–8]. Zhou et al. [9] considered the existence of train and track and analyzed the vertical dynamic interactions of the train-track-tunnel-soil coupled system by a semi-analytical approach. Analytical approach can derive the theoretical solution based on strict mathematical manipulation, but it is usually feasible to tackle with some simple cases. More researchers turn to numerical methods to reveal the train-induced vibration. Gupta et al. [10], Bian et al. [11], and Ma et al. [12] studied the train-induced vibration on a historic Bell Tower above two spatially overlapping metro lines using the 3D FE model. The above studies all treat the ground as a single-phase elastic medium; as for the saturated ground, He et al. [13,14] proposed a 2.5D FEM-BEM to investigate the responses of a metro tunnel in the saturated ground and discussed the displacements and pore water pressures under different permeability coefficients. Numerical simulation is superior to the analytical approach in revealing the train-induced vibrations and is often used as a supplement and reference to the analytical solution and field measurement. However, the present numerical study mostly regards the ground as an elastic or viscoelastic medium without considering the plastic deformation and soil-water interaction in the ground, especially in the soft deposits. Field measurement is recognized to be the most effective method to determine the train-induced vibration. A great number of field measurements have been performed to understand the vibration characteristics in the tunnel or on the ground surface [15–21]. For example, Liu et al. [19] measured the vibration accelerations of different track patterns in the metro tunnel and compared their discrepancy in vibration reduction. Zou et al. [20] measured the vibrations of ground surface and nearby buildings in the metro depot and also analyzed the changes of acceleration, vibration frequency, and sound level. Cao et al. [21] measured the vibration in a residential building on an elevated metro depot; moreover, large-scale international tests were conducted in Europe to analyze the characteristics and uncertainties in the ground-borne vibration [19]. Besides, some researchers adopted the field vibration test to verify the feasibility of a 2.5D FE-BE model based on the field measurement data [10,22]. Nevertheless, most field measurements were performed on the ground surface or in the tunnel except in the ground; thus, the response and attenuation characteristics in the ground were seldom studied. Degrande et al. [15] performed comprehensive vibration tests on the rail, tunnel invert, and in the ground and on the ground surface; however, the surrounding ground is London clay, whose mechanical property is much superior to the soft deposits. The train-induced vibration in the soft deposits is more serious and complex for it involves soil-water interaction and nonlinear deformation in the ground. Therefore, vibration measurement in the soft deposits is essential to reveal the whole responses of the tunnel-ground system. On the other hand, field measurement only measures the acceleration responses in the tunnel-ground system while the dynamic displacement and excess pore water in the soft deposits cannot be measured; as a result, numerical simulation is an important supplement to the field measurement. By combining the field measurement and numerical simulation together, the train-induced vibration characteristics from a metro tunnel in the soft deposits can be revealed in detail.

The purpose of this study was to investigate the train-induced vibration characteristics from the tunnel to the soft deposits; different from previous in-situ vibration tests, herein a comprehensive measurement was conducted by installing accelerometers in the tunnel, in the ground, and on the ground surface. Besides, numerical simulation is also performed to reveal the acceleration, displacement, and excess pore water pressure in the soft deposits based on soil-water coupled elastoplastic analysis. By analyzing the measured and calculated results, the train-induced vibration responses from a metro tunnel in the soft deposits are clarified.

2. Field Measurement

2.1. Measurement Site. Field measurement was conducted at a slightly curved section between Zui baichi Station and South Songjiang Station of the Shanghai Metro Line 9. As illustrated in Figure 1, the measured site locates at the last section of the metro line with a radius of 450 m. The surroundings are simple; there are no high buildings except some low-rise residential houses around. Soil profile at the measured site is shown in Figure 2; within a depth of 50 m, there are seven soil layers, a typical soil profile of Shanghai Yangtze delta. The metro tunnel is buried between muddy clay ④1 and clay ⑤1, with a cover depth of 13.2 m. The outer and inner radii of the tunnel are 6.2 m and 5.5 m, respectively. The water table locates at the bottom of the artificial fill, and the physical parameters of the soil layers are listed in Table 1.

2.2. Accelerometer Arrangement

2.2.1. Accelerometer Patterns. Vibration measurement was performed to investigate the response characteristics from the tunnel interior to the ground surface. Accelerometers were installed on the track, tunnel wall, in the soil layers, and on the ground surface. As shown in Table 2, the accelerometer patterns were chosen according to the vibration frequency of the track-tunnel-ground system; all the accelerometers are ICP piezoelectric accelerometers, whose work principle is the same as that of MEMS (Micro Electro Mechanical System). The electronic particles are full of the capacitive layer of the accelerometer; once train vibration happens, the electronic particles get into motion and their distribution changes, which make the voltage between the top and bottom capacitive layers change. The voltage signal is finally transformed into electrical signal after filtering and modification, and the acceleration is therefore measured.

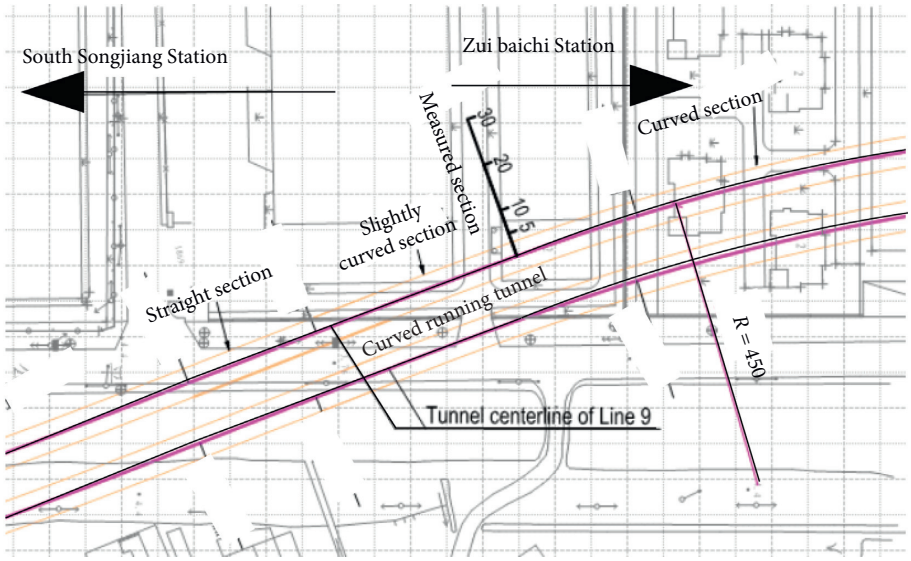

Figure 1: Planar view of the measured site.

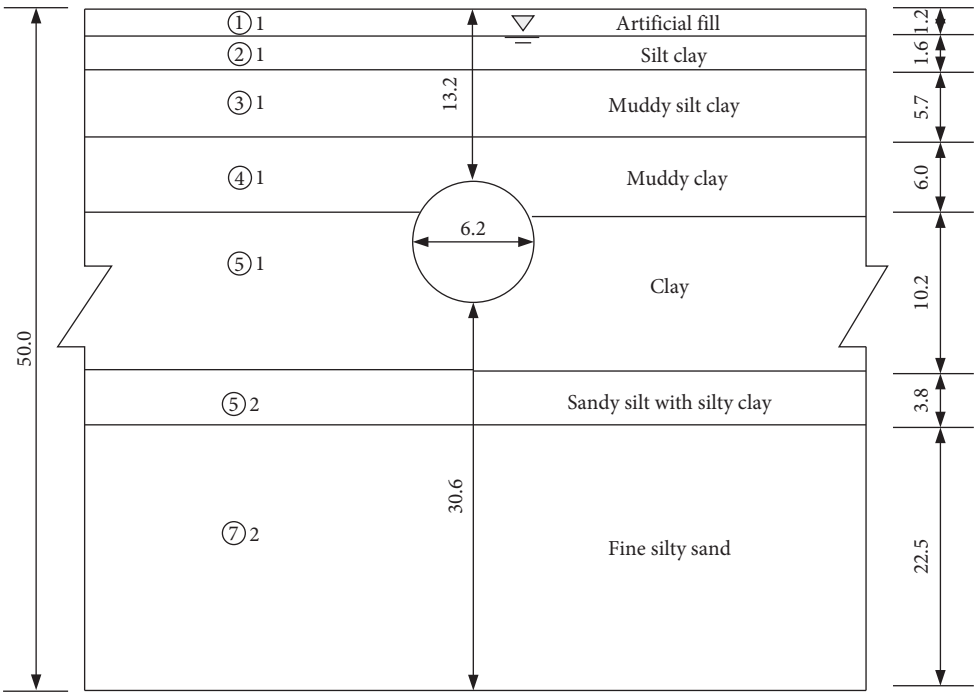

Figure 2: Soil profile at the measured site (unit: m).

2.2.2. Accelerometers in the Tunnel. Figure 3 shows the acceleration measurement points in the tunnel; there are five points in total, three at the rail, one on the track bed, and another one on the tunnel wall. Figures 4 and 5 show the in-situ arrangement of accelerometers in the tunnel; the transverse vibration of the rail waist and the vertical vibration of the rail foot as well as the vertical and transversal vibrations of the track bed and tunnel wall were measured; all the measured data were transmitted to the same data acquisition instrument.

2.2.3. Accelerometers in the Ground and on the Ground Surface. The measurement points in the soil layers and on the ground surface are shown in Figure 6. There are 31 measurement points in total—26 points buried in the soil layers and 5 points fixed on the ground surface. The measurement points in the soil layers were arranged in five columns, with respective transversal distance of 0 m, 4.65 m (0.75 D), 9.30 m (1.5 D), 12.40 m (2.0 D), and 15.50 m (2.5 D) away from the tunnel centerline, numbered by A011~A053 and 1#~3#. The points on the ground surface are fixed at a

Table 1: Physical parameters of the soil layers.

Soil type	Unit weight γ (kNm^{-3})	Initial void ratio e_{int}	Compression modulus $E_{s0.1\text{-}0.2}$ (MPa)	Poisson's ratio ν	Cohesion under CU test c_{cu} (kPa)	Friction angle under CU test φ_{cu} (°)	Permeability coefficient k (ms^{-1})	Shear velocity V_s (ms^{-2})
Artificial fill ①1	17.8	0.96	5.0	0.33	10	13	—	110
Silty clay ②1	18.6	0.86	9.0	0.32	14	12.5	$1e-7$	220
Muddy silt clay ③1	17.6	1.23	2.84	0.34	13	10	$8e-8$	150
Muddy clay ④1	16.9	0.92	2.12	0.35	12.0	10.5	$4e-8$	140
Clay ⑤1	17.5	0.82	3.13	0.33	16	12	$2e-7$	160
Sandy silt with silty clay ⑤2	18.0	0.78	5.44	0.28	12	18	$8e-7$	190
Fine silty sand ⑦2	18.7	0.68	12.82	0.26	4	30	$5e-5$	250

Table 2: The main technical index of different accelerometers.

Accelerometer types	Measured object	Sensitivity (mv/g)	Measured frequency range (Hz)	Measuring range (g)	Measured directions	Number of measurement points
LC0116TM	Ground surface	10000	0–500	0.5	Z (vertical), Y (transversal)	5
INV9828ICP	Soil layers	500	0–2500	10	Z, Y, X (longitudinal)	26
INV9822AICP	Track bed, tunnel wall	100	0–8000	50	Z, Y	2
INV9824ICP	Rail	5	0–15000	1000	Z, Y	3

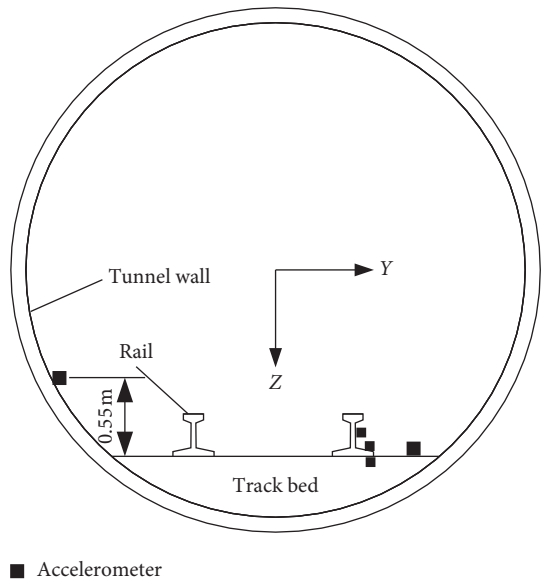

Figure 3: Diagram of measurement points in the tunnel.

distance of 0 m, 5 m, 10 m, 20 m, and 30 m away from the tunnel centerline, numbered by A01~A05. Vertical, transversal, and longitudinal vibrations were all measured for each point in the ground while only the transversal and vertical vibrations were measured for the points on the ground surface.

The accelerometers buried in the soil layers are shown in Figure 7. They were hidden in a metal box supported by a three-legged bracket; the box was filled with a foaming agent (polyurethane) to avoid water entering before burying in the ground. The three-legged bracket was put into a bored hole and sunk along the hole to a prescribed depth. The

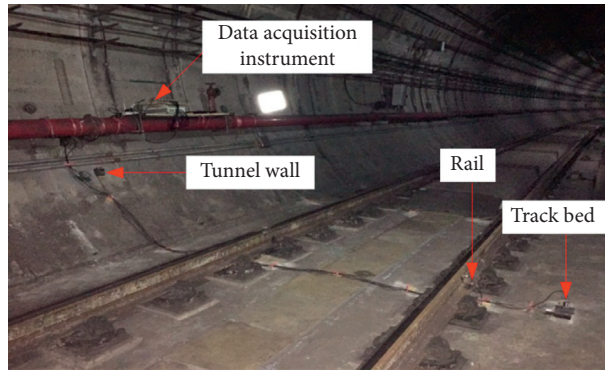

Figure 4: In-situ arrangement of accelerometers in the tunnel.

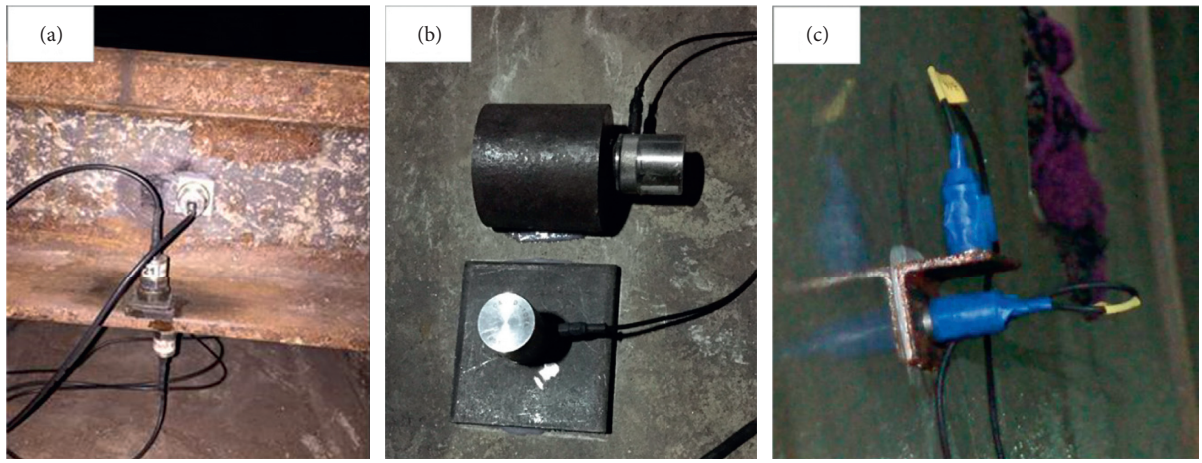

Figure 5: Accelerometers installed on the (a) rail, (b) track bed, and (c) tunnel wall.

installment of accelerometers on the ground surface is much simpler. As seen in Figure 8, the ground was flattened first, then a steel plate was placed on the ground surface as a pedestal. Two accelerometers were fixed on the steel plate to measure the transverse and vertical vibrations.

2.3. Acceleration Data Processing. Each measurement point collected 21 groups of acceleration data, the peak acceleration from each group was first determined, and then the maximum, minimum, and average peak accelerations were calculated. On the other hand, root mean square acceleration was determined to determine the vibration level of the acceleration. Finally, the frequency spectrum characteristics and vibration level under one-third octave frequency were analyzed to reveal the dominant vibration frequency in each subsystem.

According to the environmental vibration assessment standard ≪Urban Environmental Vibration Standard≫ (GB10071-88), the vibration level is an indicator to evaluate the train-induced vibration, which is calculated as follows:

$$L_a = 20\log \frac{a_e}{a_{\text{ref}}}, \tag{1}$$

where a_e is the weighted effective acceleration in m/s^2; a_{ref} is the reference acceleration, equal to 10^{-6} m/s^2. a_e is calculated as follows:

$$a_e = \sqrt{\sum_{i=1}^{n} a_{\text{rms}}^2 \cdot 10^{C_i/10}}, \tag{2}$$

where a_{rms} is the root mean square acceleration under the ith center frequency; C_i is the weight coefficient corresponding to the ith center frequency. For the measured discrete acceleration data, a_{rms} can be calculated as follows:

$$a_{\text{rms}} = \sqrt{\frac{1}{m}\left(a_1^2 + a_2^2 + \cdots + a_m^2\right)}, \tag{3}$$

where a_1 to a_m is the individual acceleration value within the ith center frequency band. As for the one-third octave frequency, the frequencies in each band are calculated as follows:

$$f_0 = \sqrt{f_1 \cdot f_2},$$
$$\frac{f_2}{f_1} = 2^{1/3}, \tag{4}$$

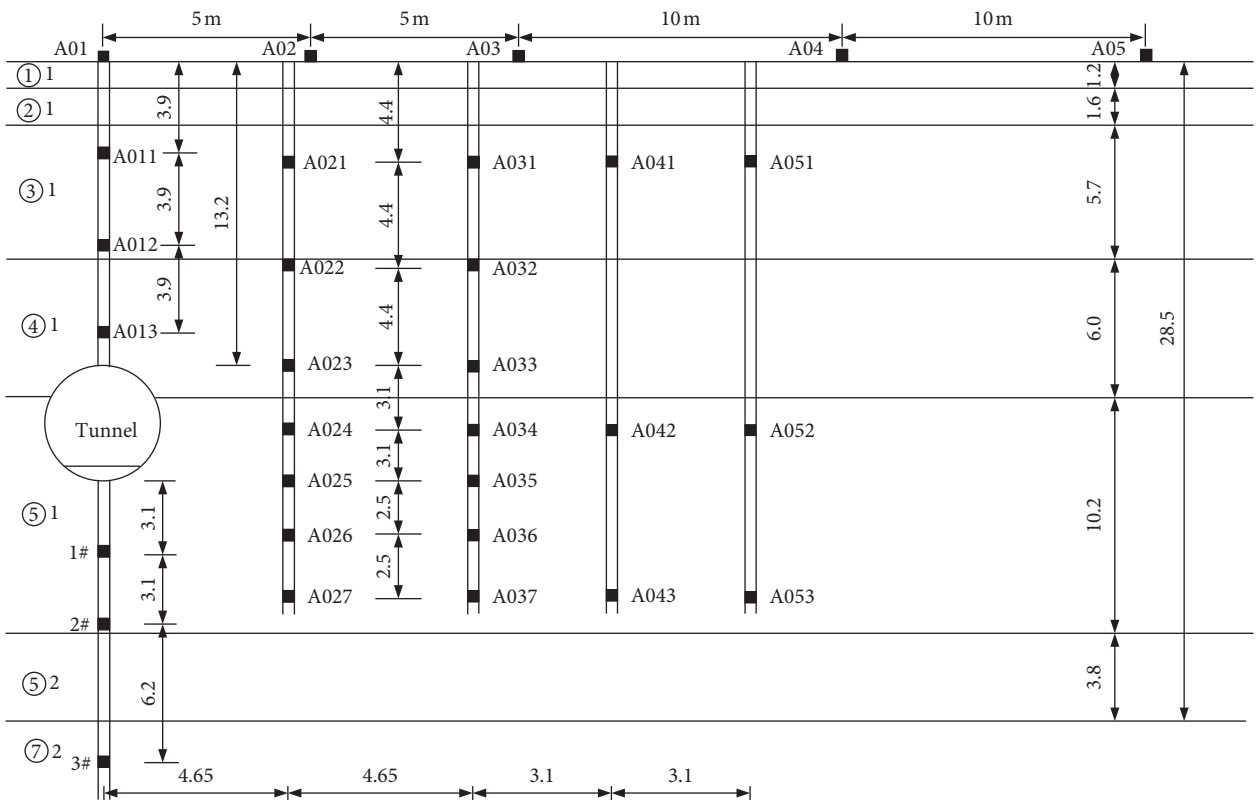

Figure 6: Diagram of measurement points in the ground and on the ground surface.

Figure 7: Accelerometer device in the ground.

Figure 8: Accelerometers installed on the ground surface.

Table 3: Peak accelerations on the track bed and the tunnel wall (unit: m/s^2).

Measurement point	Top of rail foot	Rail waist	Bottom of rail foot	Track bed		Tunnel wall	
Direction	Z	Y	Z	Z	Y	Z	Y
Maximum value	171.94	110.77	123.99	0.252	0.213	0.159	0.148
Minimum value	127.25	90.63	99.59	0.164	0.141	0.080	0.081
Average value	139.34	103.07	112.54	0.200	0.184	0.110	0.105

where f_1, f_2, f_0 are the lower, center, and upper bound frequencies, respectively.

2.4. Measurement Results and Analysis. The train-induced vibration characteristics of the track, tunnel, and ground subsystem were individually analyzed first. Based on the measured acceleration data, the peak acceleration, vibration level, and the frequency spectrum curves were all determined. By analyzing the changes of such indicators from the track to the ground surface, the whole propagation and attenuation characteristics of the track-tunnel-ground system were clarified.

2.4.1. Vibration in the Tunnel. The maximum, minimum, and average peak accelerometers of each measurement point in the tunnel are given in Table 3. It is seen that the rail's vertical acceleration is maximum, with an average peak value of 139.34 m/s^2. Nevertheless, due to the curvature of the tunnel, the transverse acceleration of the rail is high at 103.07 m/s^2, implying that the curvature of the tunnel can induce significant transversal vibration in the tunnel. The train-induced vibration experiences the first attenuation from the top of the rail foot to its bottom, since its acceleration drops from 139.34 m/s^2 to 112.54 m/s^2. When vibration transmits to the track bed, the acceleration response is dramatically attenuated for the maximum vertical and transversal accelerations to drop to 0.252 m/s^2 and 0.213 m/s^2, respectively. The accelerations of rail and track bed actually belong to different orders of magnitude. The reason is that the rail is connected with the track bed by a discrete rail pad while the track bed is fixed with the metro tunnel, so the rail vibrates violently while the vibration of the track bed is significantly reduced. When the vibration propagates to the tunnel wall from the track bed, the decrease of accelerations is slight.

The time history curves of vertical acceleration in the tunnel are illustrated in Figure 9. It clearly shows that the rail's acceleration changes are more drastic than the track bed and the tunnel wall. There are significant impulses in the time history curves of rail, which overall corresponds to the passing of the train's wheelsets. As for the track bed and the tunnel wall, the fluctuation is much gentler without apparent impulse. Therefore, the time history curve also indicates that great attenuation takes place when vibration propagates from the rail to the track bed, while there is a slight decrease from track bed to the tunnel wall. The accelerations of rail and track bed belong to two orders of magnitude, but the accelerations of the track bed and tunnel wall are approximate to each other.

2.4.2. Ground-Borne Vibration. Considering the number of accelerometers and the large amount of data, herein only some representative points are selected for analysis. The accelerations of 1#~3# reflect the ground vibration below the tunnel while the accelerations of A021~A027 represent the ground vibration beside the tunnel; so points 1#~3# and A021~A027 are selected here for the following analysis.

(1) Peak Acceleration. The average peak accelerations of 1#~3# points in the three directions are listed in Table 4. It is seen that the vertical accelerations are far larger than the accelerations in the other two directions. The maximum vertical acceleration locates at the bottom of the tunnel, at about 0.32 m/s^2. Due to tunnel curvature, the transversal and longitudinal accelerations still exist rather than zero. The time history curves of vertical acceleration of 1#~3# are presented in Figure 10 . The peak acceleration decreases with the increase of depth; moreover, the number of acceleration impulse is also diminished, which also implies that the vibration frequencies are attenuated during the propagation process.

As for points A021~A027, their average peak accelerations are shown in Table 5. It is seen that the vertical acceleration is also much larger than the transversal and longitudinal accelerations, which confirms that the vertical vibration is still the dominant ground vibration. The acceleration changes of A021~A027 with the depth are illustrated in Figure 11 The vertical acceleration first increases with the depth until it reaches a peak at the spring line, then the vertical acceleration starts to decrease as the depth continues to increase. The changes of accelerations in the Y direction and X direction are similar but different from the changes of vertical acceleration. There are two peaks for the transversal or longitudinal accelerations, which are located at the upper and lower haunches of the tunnel. In other words, there is amplification phenomenon in the ground for the transversal and vertical accelerations; this phenomenon was seldom found in the previous field measurement since field measurement was rarely conducted in the soil layers. In sum, the vertical vibration is still dominant among the ground vibrations near the tunnel, and the transverse and the longitudinal vibrations are approximate; the transversal acceleration is slightly larger than the longitudinal within the depth of the tunnel due to tunnel curvature. When the measurement points are far from the tunnel, however, the ground accelerations in the three directions are similar to each other.

Similarly, the acceleration time history curves in the ground can be depicted. Take A021, A024, and A027 for example; the time history curves of vertical and transversal

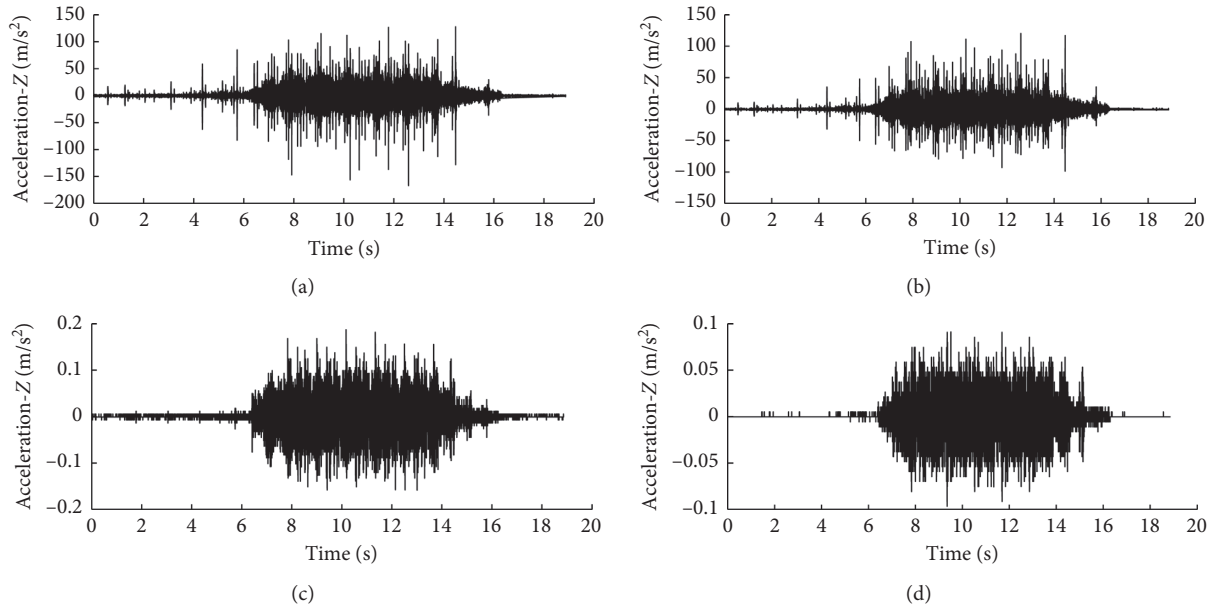

Figure 9: Time history curves of vertical accelerations: (a) top of the rail foot; (b) bottom of the rail foot; (c) track bed; (d) tunnel wall.

Table 4: Average peak accelerations of 1#~3# (unit: m/s^2).

Points	1#			2#			3#		
Direction	Z	Y	X	Z	Y	X	Z	Y	X
Average value	0.287	0.097	0.092	0.165	0.072	0.079	0.135	0.071	0.073

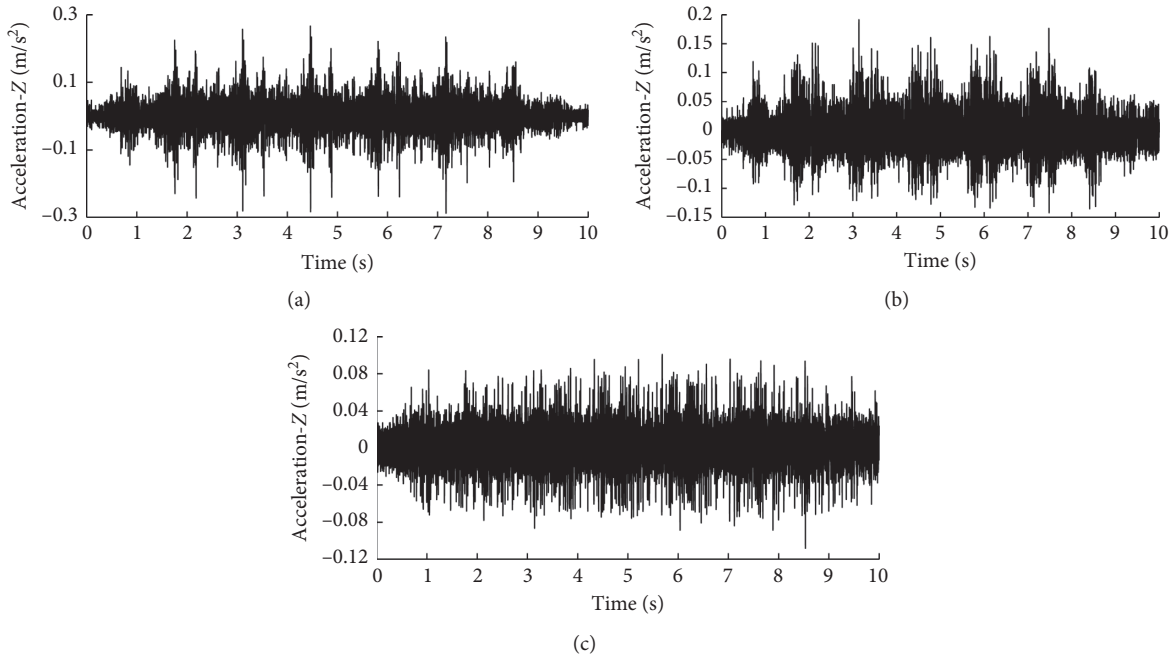

Figure 10: Time history curves of vertical accelerations: (a) 1#; (b) 2#; (c) 3#.

accelerations are shown in Figures 12 and 13. It is clearly seen that the closer to the tunnel, the stronger the ground vibration, with larger accelerations and more fluctuations in the time history curves. A024 is the closest point to the tunnel, so its vibration response is particularly violent, with many visible impulses. As for A021 and A027, their

Table 5: Average peak accelerations of A021~A027 (unit: m/s^2).

Point	A021	A022	A023	A024	A025	A026	A027
Depth (m)	−4.4	−8.8	−13.2	−16.3	−19.4	−21.9	−24.4
Accl-*Z*	0.161	0.172	0.235	0.296	0.273	0.187	0.113
Accl-*Y*	0.052	0.058	0.156	0.086	0.058	0.184	0.065
Accl-*X*	0.058	0.062	0.182	0.035	0.051	0.145	0.081

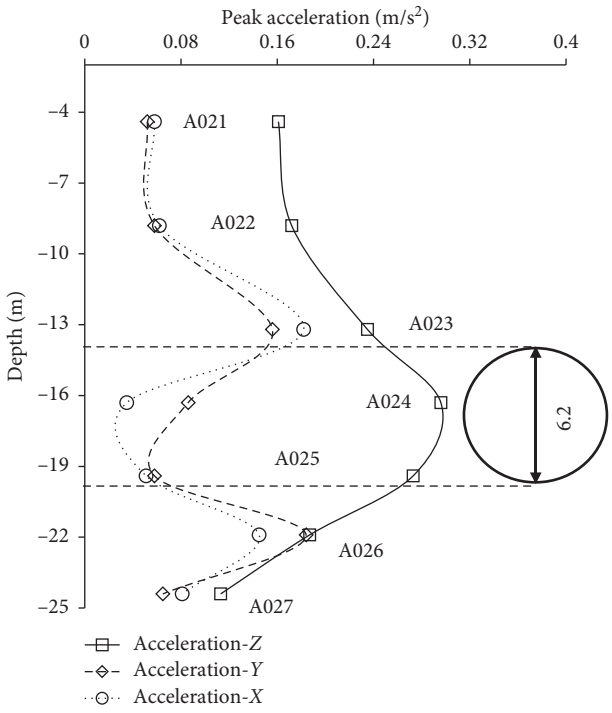

Figure 11: Distribution of accelerations along the depth direction at A021~A027.

responses are much milder, which actually relates to the decrease of vibration frequency.

The average peak accelerations on the ground surface are listed in Table 6. The measured maximum vertical and transversal accelerations are 0.235 m/s^2 and 0.189 m/s^2, respectively. It is found that the peak acceleration decreases rapidly in the transversal direction, and the attenuation rate of vertical acceleration is much larger than that of the transversal acceleration. Besides, there are also acceleration amplification areas on the ground surface, at a distance of 20–30 m away from the tunnel center. The acceleration amplification is mainly induced by the superimposed effect of Rayleigh wave and body waves on the ground surface, which was also confirmed by other researchers [18]. In addition, the measured results show that the acceleration of A01 is larger than that of A011; therefore, the acceleration seems to increase as the ground vibration transmits to the ground surface. Such phenomenon is also rarely mentioned in the previous measurement, so it needs to be further clarified by the numerical simulation. Similarly, the time history curves of representative points on the ground surface are illustrated in Figure 14.

Based on the average peak accelerations of all the measurement points in the ground, the acceleration contours on the cross section can be depicted as in Figure 15. Since acceleration contour in the *X* and *Y* directions are similar, only the vertical and transversal acceleration contours are presented here. It is clearly seen that acceleration contours in the *Z* and *Y* directions differ significantly, and the maximum vertical acceleration locates at the bottom of the tunnel, and attenuates like an arc in the transversal direction. Within the transversal distance of 30 m, the vertical acceleration attenuates from 0.32 m/s^2 to 0.02 m/s^2. As for the transverse acceleration, the maximum transverse acceleration does not locate at the spring line but appears at a distance from the tunnel. As seen in Figure 15(b), amplification phenomenon appears at the upper and lower haunches of the tunnel, about 45° above and below the spring line, respectively. In the range of 30 m away from the tunnel, the transverse acceleration attenuates from 0.22 m/s^2 to 0.02 m/s^2.

2.4.3. Vibration Level under One-Third Octave Frequency. The vibration level based on the root mean square acceleration was also calculated. The vibration levels from the measurement points in the tunnel are presented in Table 7. It indicates that the changes of the vibration level are consistent with the changes of peak acceleration. The average vertical vibration level on the top of the rail foot is 141.63 dB while the counterparts of the track bed and the tunnel wall are only 89.21 dB and 84.21 dB, respectively, a 37% decrease from the rail to the track bed. Due to tunnel curvature, the transversal vibration level is also significant; the vibration levels from the rail waist, track bed, and tunnel wall are 135.06 dB, 88.26 dB and 83.60 dB, respectively.

Figure 16 illustrates the vibration level under the one-third octave frequency in the tunnel. It is found that the vibration frequency band of rail is broad, ranging from 0 Hz to 2500 Hz, and the rail's dominant frequency mainly concentrates in the high frequency band, with a peak frequency of 1250 Hz. As for the track bed and the tunnel wall, the frequency bands are also wide, but the high frequency contents are significantly attenuated. The dominant frequency band concentrates in the range of 25–400 Hz with two peak frequencies at 31.5 Hz and 125 Hz. The first frequency is close to the natural frequency of the tunnel-ground model and the second peak frequency is approximate to the natural frequency of the rail-track model. It is seen that there remains some high frequency contents in the *Y* direction for the track bed, which is likely related to the horizontal roughness of the rail induced by corrugation.

The vertical vibration levels of 1#~3# are shown in Figure 17 . The dominant vibration frequency bands of the three points are similar, ranging from 20 Hz to 200 Hz. The

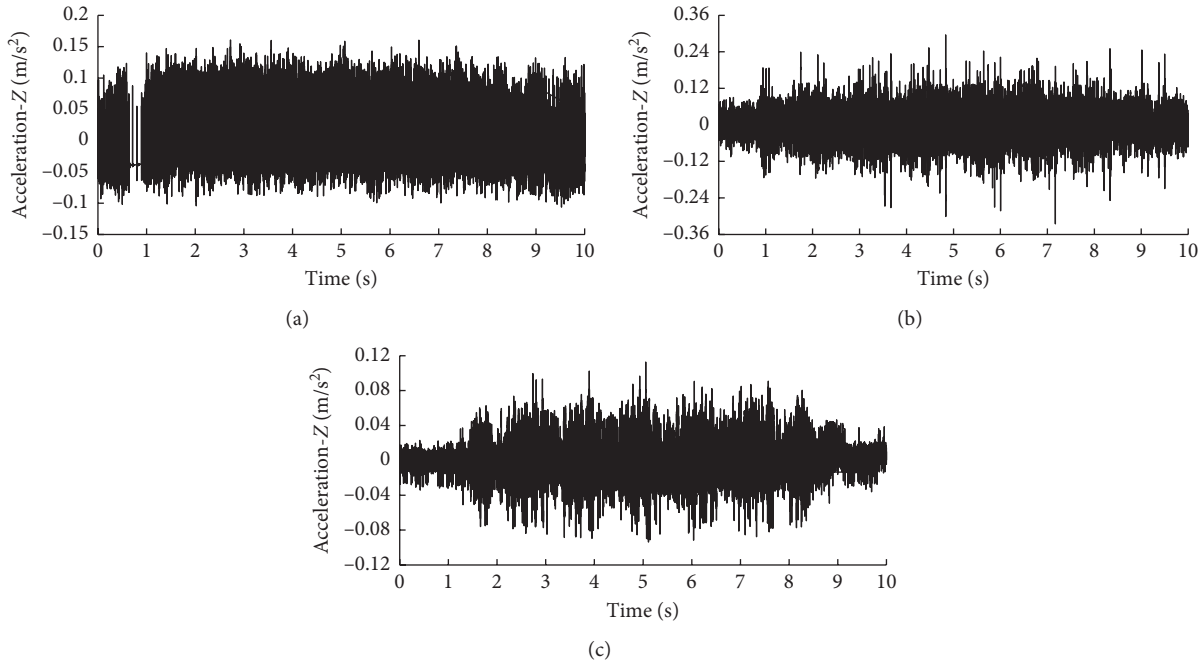

Figure 12: Time history curves of vertical accelerations: (a) A021; (b) A024; (c) A027.

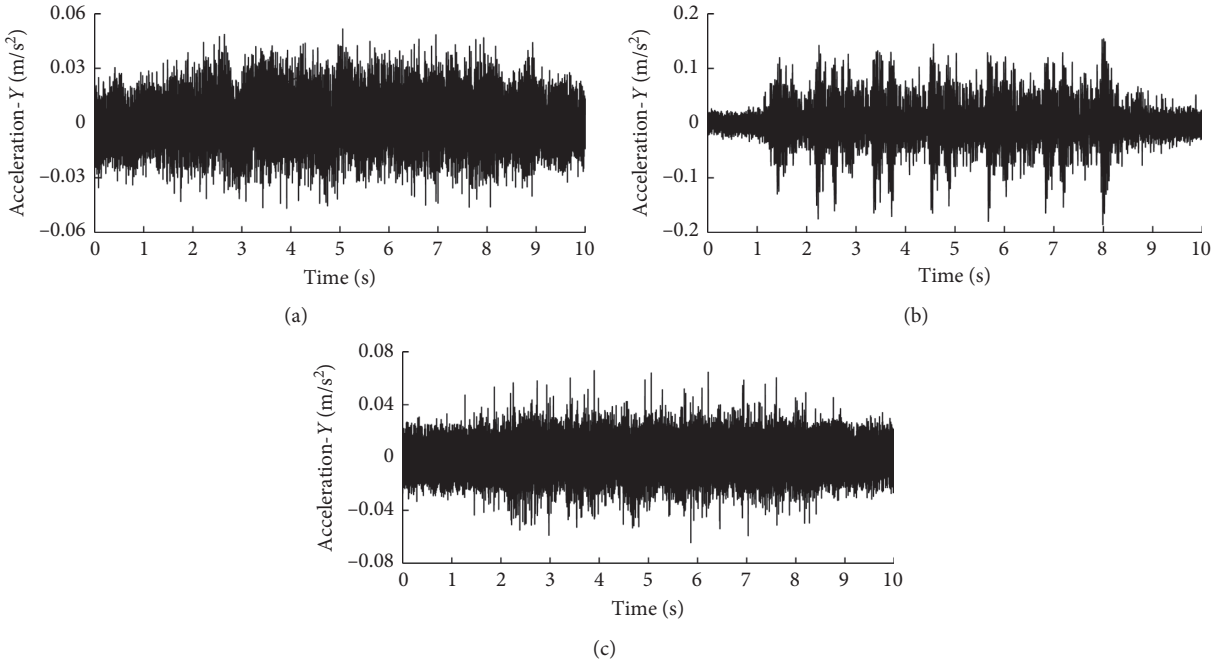

Figure 13: Time history curves of transversal accelerations: (a) A021; (b) A024; (c) A027.

vibration level still peaks at frequencies of 31.5 Hz and 125 Hz on the track bed and tunnel wall. By comparing the vibration frequencies between the soft ground and the track, it is concluded that the high frequency components are greatly attenuated when the train-induced vibration transmits to surrounding soft deposits from the tunnel interior.

Similarly, the vibration levels of A01~A05 are shown in Figure 18. It is shown that the changes of vibration level are similar for the five points. The high frequency contents have been further diminished when vibration transmits to the ground surface; overall, the dominant high frequency band concentrates in the range of 20–100 Hz. Vibration levels of A01~A05 also peak at 31.5 Hz, but the vibration level decreases rapidly as the frequency exceeds the peak frequency. The dominant frequency band is found to be similar to the measurement results from other researchers that the train-

Table 6: Average peak accelerations on the ground surface (unit: m/s^2).

Measurement points	A01	A02	A03	A04	A05
Acceleration-Z	0.235	0.137	0.033	0.021	0.026
Acceleration-Y	0.189	0.126	0.072	0.062	0.068

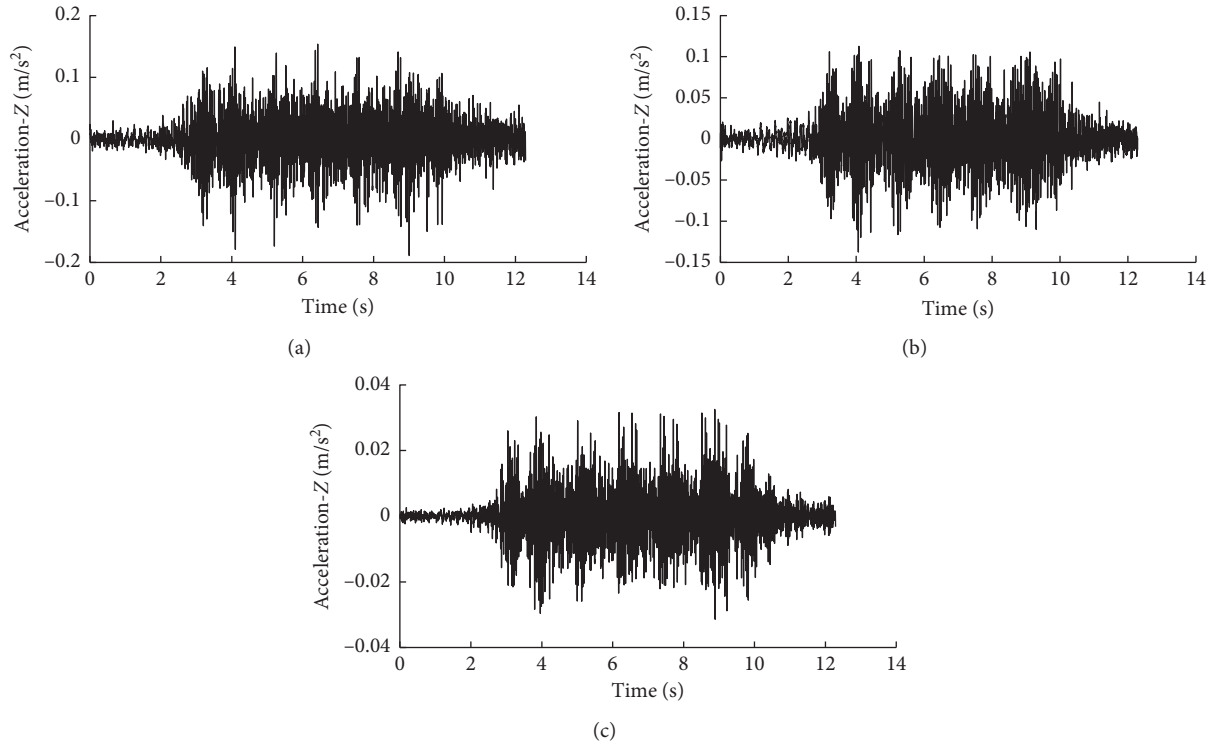

Figure 14: Time history curves of vertical on the ground surface: (a) A01; (b) A02; (c) A03.

induced vibration frequency on the ground surface is assumed to be about 20–80 Hz [18,23,24], so the field measurement outcomes in this study are rational.

2.4.4. Frequency Spectrum of the Track-Tunnel-Ground System. By making Fourier Transformation on the time history data of acceleration, the frequency spectrum characteristics of the track-tunnel-ground system can be determined. Figure 19 shows the frequency spectra of vertical acceleration at different locations. It also proves that the vibration frequency experiences apparent attenuation from the rail to the ground surface. The vibration frequency of the rail is broad, and the dominant frequency bands focus in 100–400 Hz and 1000–1500 Hz. When the vibration transmits to the track bed and the tunnel wall, the high frequencies are significantly decreased; the frequency drops to below 500 Hz. As the vibration transmits to the surrounding soil layers, the vibration frequency attenuates further due to ground damping; the dominant frequencies are overall less than 400 Hz, as seen in the A024 and 1#, and the dominant frequency is even less than 200 Hz. Finally, when the vibration reaches the ground surface, the vibration frequency decreased to 0–100 Hz, as illustrated at A01. In sum, the dominant frequency at the different subsystems is different, and the high frequency contents are greatly attenuated in the propagation process. Determining the vibration frequencies from the tunnel to the ground surface has an important reference value to the analytical or numerical study on the train-induced environmental vibration.

3. Numerical Simulation

The field measurement generally obtains the acceleration response of the track-tunnel-ground system; however, for the metro tunnel in the soft deposits, dynamic displacement and pore water responses should also be paid attention. Therefore, numerical simulation is a favorable supplement to understand all the train-induced response characteristics, including the acceleration, displacement, and excess pore water pressure responses in the coupled system. Since the soft ground consists of saturated soil layers, herein elasto-plastic soil model and soil-water coupled theory were considered in the numerical simulation. The train vibration load on the track bed was determined by the track-tunnel-ground analytical model. Finally, three-dimensional dynamic calculation was performed to obtain the acceleration, displacement, and excess pore water pressure responses

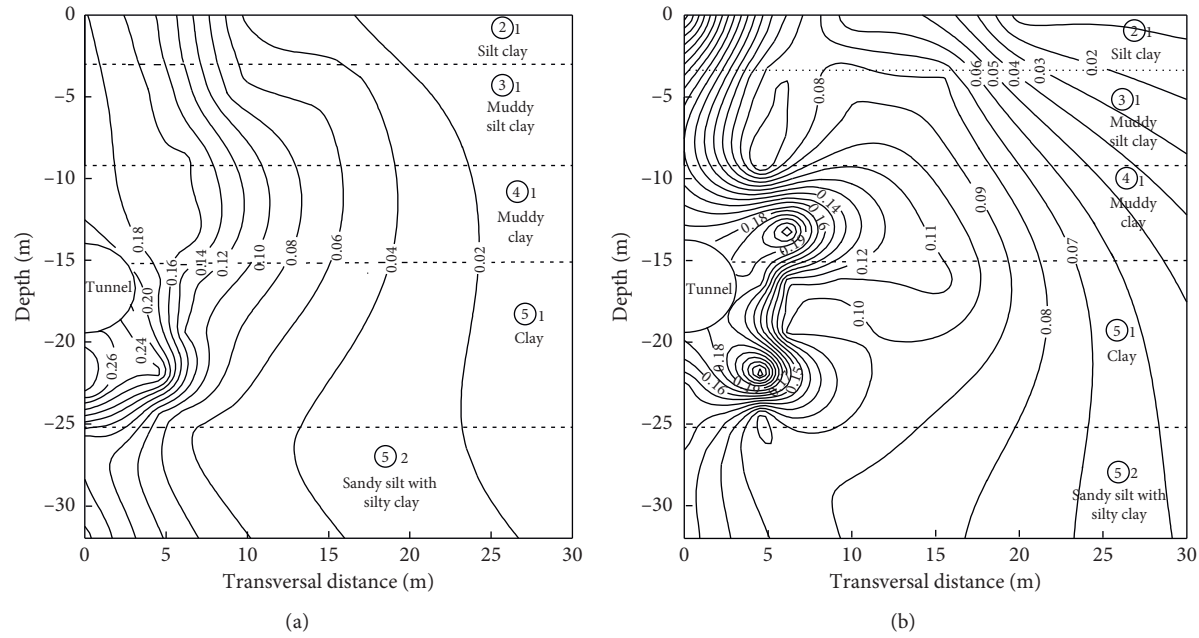

Figure 15: Acceleration contour of surrounding soil layers: (a) Z direction; (b) Y direction.

Table 7: Vibration levels at measurement points in the tunnel (unit: dB).

Location	Top of rail foot	Rail waist	Bottom of rail foot	Track bed		Tunnel wall	
Direction	Z	Y	Z	Z	Y	Z	Y
Maxima	142.50	137.10	140.99	89.83	89.34	85.65	84.84
Minima	140.00	133.78	138.94	87.39	85.86	82.50	82.69
Average	141.63	135.06	140.42	89.21	88.26	84.21	83.60

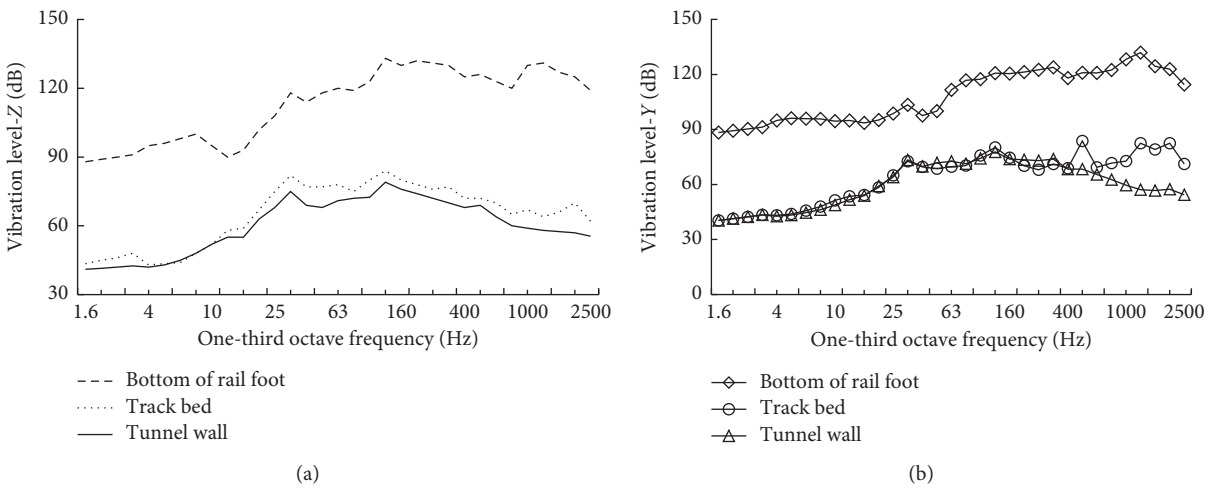

Figure 16: Vibration levels under one-third octave frequency in the tunnel: (a) Z direction; (b) Y direction.

based on soil-water coupled elastoplastic analysis using finite element-finite difference scheme (FE-FD scheme) and the program code DBLEAVES [25].

3.1. Numerical Model. The 3D model was established based on the measurement site of the Shanghai Metro Line 9, as seen in Figure 20. The size of the 3D model is

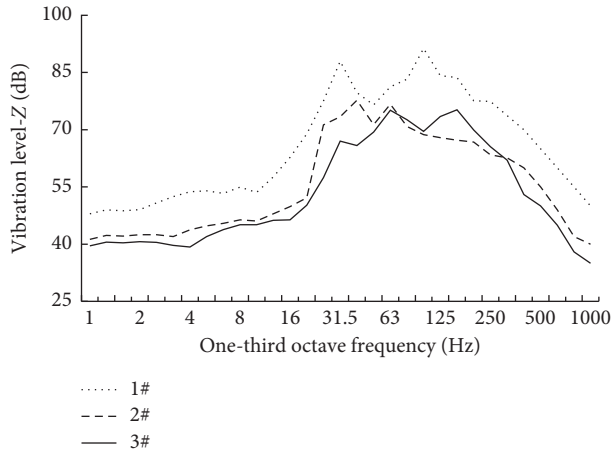

Figure 17: Vertical vibration levels of 1#~3# under one-third octave frequency.

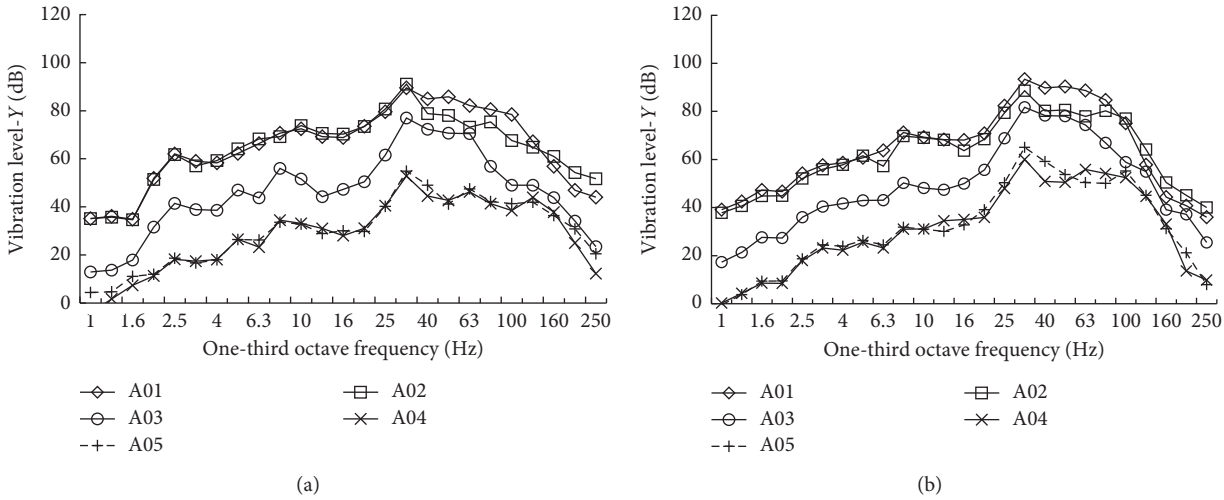

Figure 18: Vibration levels of ground surface points: (a) Z direction; (b) Y direction.

124 m × 50 m × 80 m. For simplicity, the curvature of the metro tunnel is neglected; meanwhile, only one tunnel is considered in the model since the spacing between the up line and the down line exceeds fourfold the tunnel diameter, and the dynamic interferences between the two tunnels are weak. The longitudinal cut-off length is 80 m and is divided into 40 meshes; it is found that 80 m is adequate to analyze the dynamic response of the tunnel in the soft deposits [26]. The lateral boundaries are viscous boundaries modeled with dashpots, whose normal and tangential stiffness are determined according to the formulas proposed by Lysmer and Kuhlemeyer [27]. The bottom boundary is fixed while the top is free. As for the drainage conditions, the lateral boundaries and the phreatic surface are permeable and the bottom is impermeable. A 3D model consists of hexahedron solid elements; the tunnel lining was simplified as a solid homogenous loop, and the tunnel lining and track bed are made of concrete C25 and C50, with a Young's modulus of 28.0 GPa and 34.5 GPa, respectively.

3.2. Train Vibration Load. The train vibration load was determined based on the track-tunnel-ground analytical model, as illustrated in Figure 21. The rail and the tunnel (track bed included) are modelled by Euler beam; the rail pad and the ground are modeled by spring and dashpot, with a spacing of 0.6 m; and the metro train is simplified as a series of moving point loads. Parameters of the track-tunnel-ground analytical model are listed in Table 8.

The train vibration load on the track bed is illustrated in Figure 22. The train moves at a speed of about 60 km/h; each metro train consists of six carriages, so it takes 8.36 seconds for a train passes through the tunnel. As shown in Figure 23, the train vibration load is applied on both sides of the track bed with respective phase difference along the longitudinal direction, so the total vibration time is 13.16 seconds as the train moves from $x = 0$ m to $x = 80$ m.

3.3. Constitutive Model. The cyclic mobility model is used to describe mechanical property of the soft deposits in the

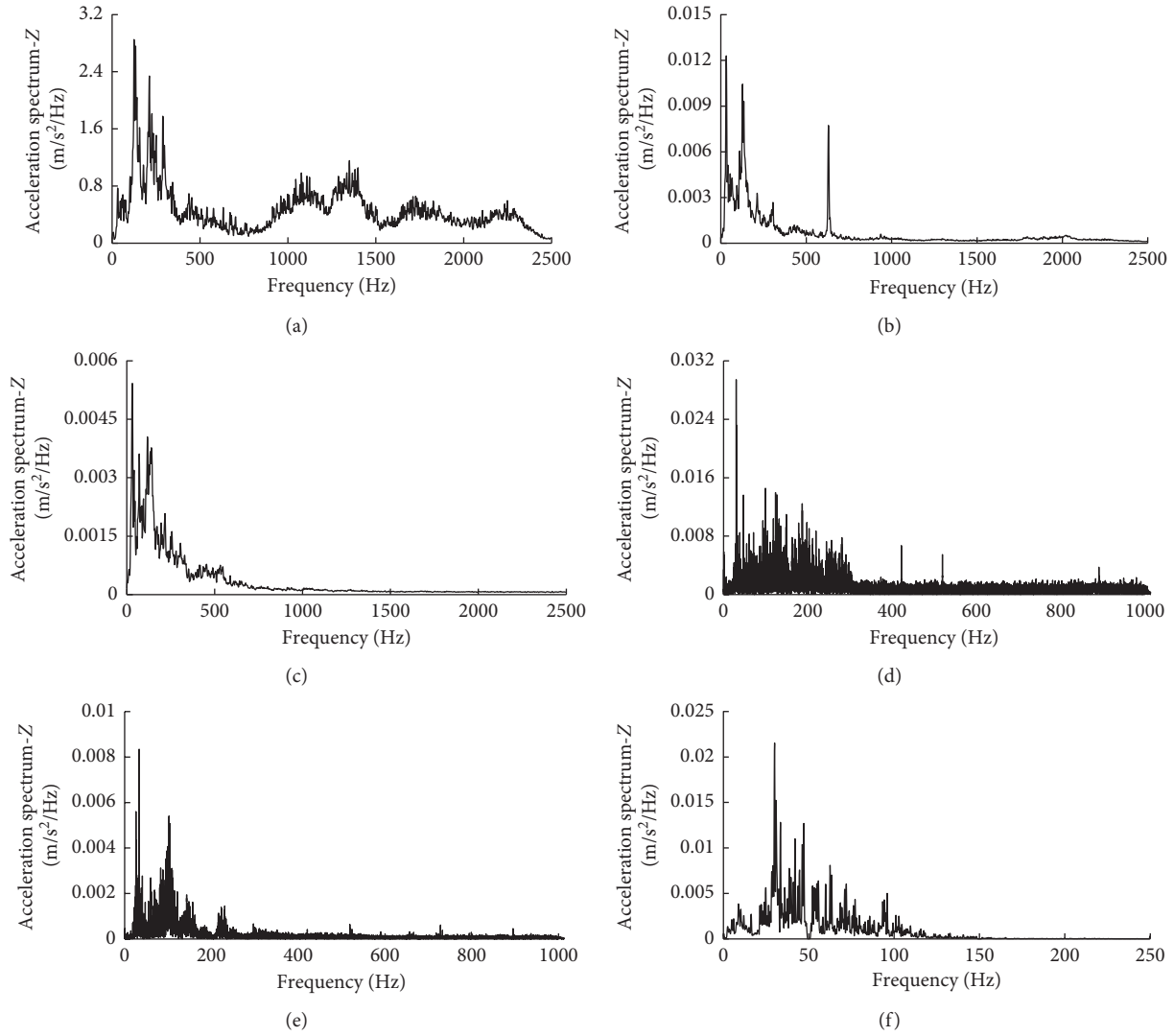

Figure 19: Frequency spectrum curves of the vertical acceleration: (a) rail foot; (b) track bed; (c) tunnel wall; (d) A024; (e) 1#; (f) A01.

study [28]. This model is an elastoplastic model based on the concepts of subloading and superloading yield surfaces, considering the stress-induced anisotropy [29,30]. There are eight parameters in the model, in which λ, κ, M, ν, and e_0 are the same as the parameters in the Cam-clay model; the other three parameters are m, a, b_r, corresponding to the loosing rate of the over-consolidation ratio, the collapse rate of soil structure, and the developing rate of stress-induced anisotropy, respectively. A significant advantage of this soil model is that static and dynamic properties of the soft deposits can be modelled with the same parameters. Currently, the model has been widely adopted in the dynamic numerical analysis of geotechnical engineering, as the feasibility and reliability of the cyclic mobility model has been validated [31–33]. As for the model parameters of the soft deposits, they have been determined by the laboratory tests, as listed in Table 9 [34]. The backfilled soil layer is regarded as an elastic layer, with Young's modulus of 15 MPa and Poisson's ratio of 0.30.

3.4. Numerical Results

3.4.1. Dynamic Responses of the Tunnel. As seen in Figure 24, T11~T15 and T21~T25 are the representative nodes of the tunnel extrados and intrados, respectively. T26 and T27 are nodes on the track bed, besides T27 is also the mode where the train vibration load applies. The calculated results of the selected points are listed in Table 10. It is seen that the maximum vertical acceleration and transversal acceleration at T26 and T23 are 34.7 cm/s^2 and 10.6 cm/s^2, respectively. The vertical peak accelerations at the tunnel invert, spring line, and tunnel crown are 34.7 cm/s^2, 24.5 cm/s^2, and 17.5 cm/s^2, respectively. It indicates that there is vibration attenuation from the tunnel invert to the tunnel crown. As for transversal acceleration of the tunnel, take T21~T25 for example; the transversal acceleration increases from the tunnel crown and reaches the maximum value at the spring line, and then decreases from the spring line to the tunnel invert. Therefore, the vibration attenuation laws of vertical acceleration and transversal acceleration in the tunnel are

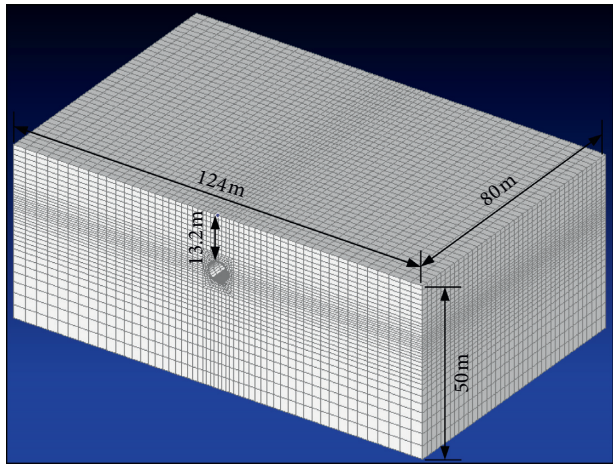

Figure 20: The 3D numerical model.

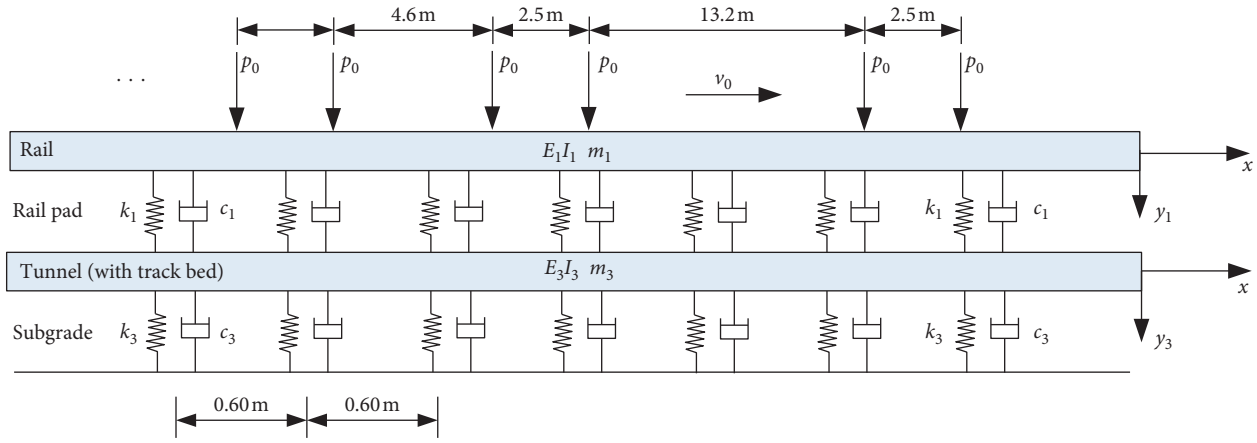

Figure 21: Track-tunnel-ground analytical model.

Table 8: Parameters of the track-tunnel-ground model.

E_1I_1 (Nm^2)	m_1 (kg/m)	k_1 (N/m^2)	c_1 (Ns/m^2)	E_3I_3 (Nm^2)	m_3 (kg/m)	k_3 (N/m^2)	c_3 (Ns/m^2)	p_0 (kN)
6.145*e*6	60.34	8*e*7	5*e*4	1.79*e*11	19970	3.5*e*6	5.0*e*4	80.0

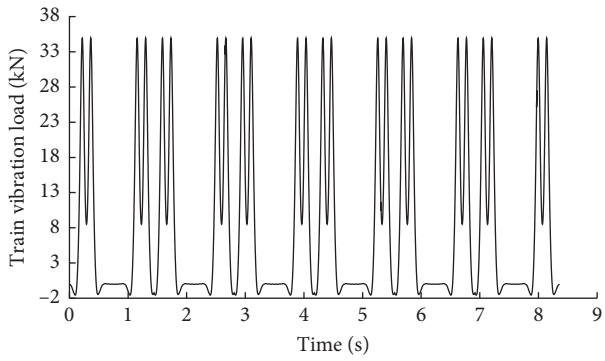

Figure 22: Time history of the train vibration load on the track bed.

totally different. Besides, the acceleration also experiences a slight decrease from the tunnel intrados to extrados. As for the tunnel vibration level, the maximum vertical and transversal vibration levels are 81.88 dB and 72.88 dB, respectively, situated at the bottom and the springline of the tunnel, respectively. In sum, by numerical calculation, the attenuation characteristics in the tunnel are revealed.

3.4.2. Responses of the Soft Deposits. By calculating the peak ground accelerations of 127 points in an area of 40 m × 35 m, the acceleration contour was plotted as shown in Figure 25. It is seen that the calculated maximum vertical and transverse accelerations in the ground are 34.5 cm/s^2 and 13.5 cm/s^2 compared to the measured 0.32 m/s^2 and 0.22 m/s^2; therefore, the calculated vertical acceleration is similar to the measured value while the calculated transverse acceleration is smaller. The reason is that the tunnel curvature is not considered in the numerical simulation for simplicity. The numerical results reveal that the maximum vertical acceleration takes place at the bottom of the tunnel and the

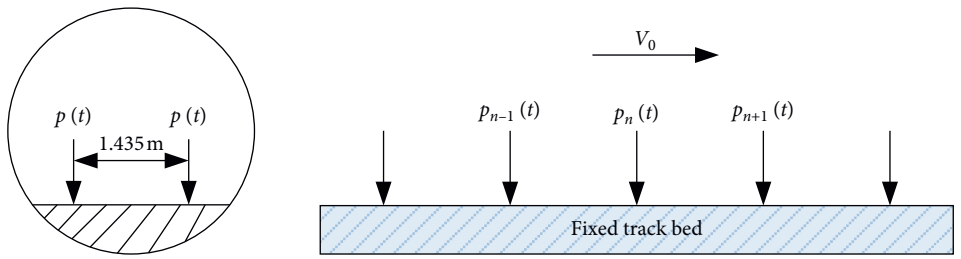

Figure 23: Diagram of train vibration load on the track bed.

Table 9: Parameters of soft soil layers [34].

Soil layers	②1	③1	④1	⑤1	⑤2	⑦2
Compression index λ	0.087	0.132	0.14	0.135	0.122	0.062
Swelling index κ	0.02	0.02	0.02	0.019	0.018	0.012
Stress ratio of critical state M	1.20	1.30	1.30	1.40	1.36	1.40
Failure ratio R_f	3.00	3.29	3.29	3.67	3.50	3.67
Void ratio e_0 (p_0' = 98 kPa on the N.C.L)	0.756	1.08	0.86	0.815	0.805	0.762
Poisson's ratio ν	0.32	0.38	0.38	0.35	0.34	0.3
Degradation parameter of consolidation m	40.0	80.0	100.0	60.0	60.0	0.50
Degradation parameter of structure a	0.30	0.1	0.1	0.10	0.1	2.5
Evolution parameter of stress-induced anisotropy b_r	0.05	0.01	0.01	0.01	0.02	1.50
Initial structure ratio R_0^*	0.8	0.30	0.20	0.60	0.40	0.70
Initial overconsolidation ratio OCR ($1/R_0$)	10.0	2.25	2.35	2.50	5.25	30.0
Initial anisotropy ζ_0	0.00	0.00	0.00	0.00	0.00	0.00

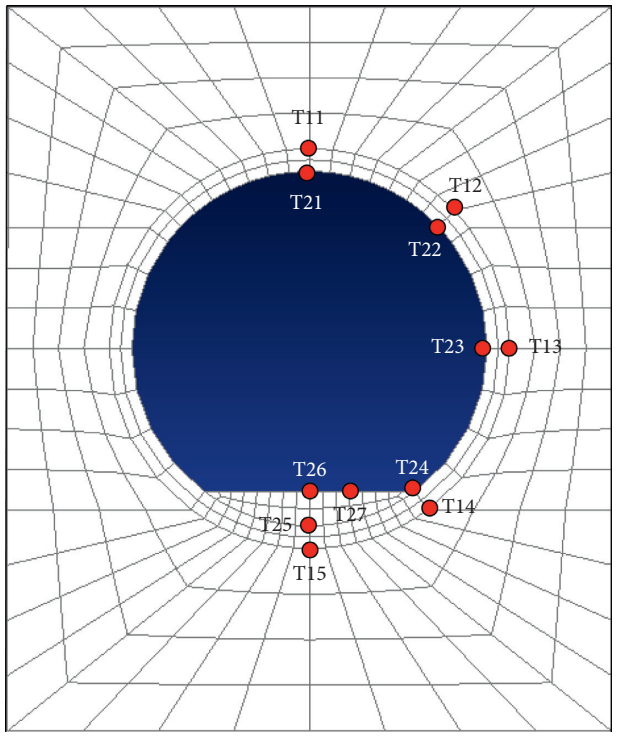

Figure 24: Representative nodes on the track bed and the tunnel wall.

vertical peak acceleration attenuates like an arc in the transverse direction. Moreover, it is found that there are also transversal acceleration amplification phenomena at the upper haunch and the lower haunch of the tunnel, as seen in Figure 25. The maximum transversal acceleration of the tunnel is 10.7 cm/s^2, while the maximum value in the ground is 13.5 cm/s^2, which confirms that the transversal acceleration increases from the tunnel interior to the surrounding ground. The numerical results reveal that there are amplification areas on the ground surface, at a distance about 20–30 m away from the tunnel, which is also consistent with the measured results. In addition, it is also found that the acceleration experiences slightly increase when the vibration propagates from the underlying saturated ground to the single-phase ground. On the top of tunnel, the vertical acceleration at $z = -1.5$ m is 2.02 cm/s^2 while the corresponding value on the ground surface is 2.28 cm/s^2. As shown in Figure 25, it is found that the acceleration attenuates rapidly in the soil layers, and the train-induced vibration effect mainly concentrates in the domain of 30 m, in which 90% of the acceleration are attenuated.

The calculated dynamic displacement contour of the soft deposits is shown in Figure 26. The dynamic displacement contour is similar to the acceleration contour, and the maximum vertical and transverse displacements are 0.42 cm and 0.16 cm, respectively. The vertical displacement attenuates like an arc in the transversal direction. For example, the vertical displacement decreases to 0.04 cm at the horizontal distance of 10 m away from the tunnel center, only 10 percent of the maximum vertical displacement. As for the transversal displacement, there exist amplification zones, appearing at the upper and the lower haunches of the tunnel, which is consistent with the case of transversal acceleration.

3.4.3. Excess Pore Water Pressure around the Tunnel. The excess pore water pressure (EPWP) distribution around the

Table 10: Response results at nodes in the tunnel.

Nodes	Acceleration-Y (cm/s^2)	Acceleration-Z (cm/s^2)	Displacement-Y (cm)	Displacement-Z (cm)	Vibration level-Y (dB)	Vibration level-Z (dB)
T26	0.00	34.70	0.00	0.42	—	81.88
T27	0.81	34.60	0.00	0.42	49.18	81.81
T11	0.00	17.40	0.00	0.39	—	74.56
T21	0.00	17.50	0.00	0.39	—	74.59
T12	4.60	23.50	0.01	0.40	66.06	77.76
T22	5.68	22.60	0.02	0.40	67.83	77.26
T13	10.70	24.50	0.03	0.40	72.88	78.38
T23	10.60	24.60	0.03	0.40	72.85	78.38
T14	0.23	29.00	0.00	0.41	39.77	80.40
T24	2.09	30.30	0.00	0.41	57.86	80.78
T15	0.00	34.50	0.00	0.42	—	81.84
T25	0.00	34.70	0.00	0.42	—	81.88

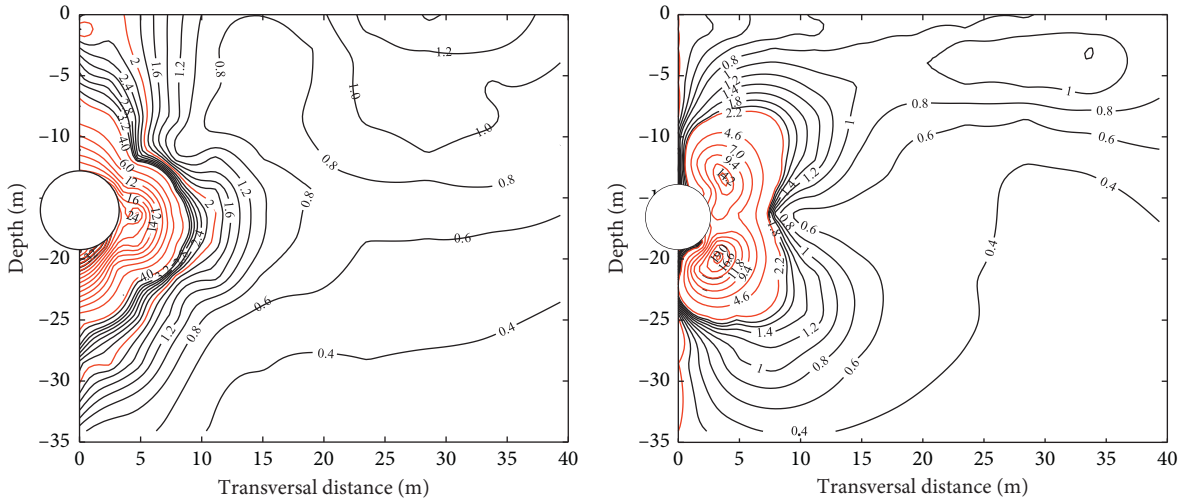

Figure 25: Acceleration contour of the soft ground: (a) vertical direction; (b) transversal direction (unit: cm/s^2).

tunnel can also be calculated using DBLEAVES. As illustrated in Figure 27, the EPWP distribution from 0° to 180° is depicted, and the other half distribution from 180° to 360° is the same. The angle θ starts from the tunnel crown and rotates in the clockwise direction. The peak EPWP response during train vibration and accumulated EPWP after train vibration are both presented. It is seen that peak EPWP at the 45° and 135° positions are much larger than other places, and the calculated maximum EPWP is 1.20 kPa, which is very close to the 1.15 kPa measured in the Shanghai metro Line 2 [35], which indicates that the numerical calculation based on soil-water coupled analysis is rational. Furthermore, it is found that there is slight EPWP accumulation after each train vibration; for example, the maximum accumulated EPWP is 0.65 kPa in Figure 27. As a result, significant EPWP will be accumulated in the soft deposits after repeated train vibrations in the long term. However, when the EPWP dissipates, the tunnel settlement takes place, which inevitably threatens the normal operation of a metro tunnel. Therefore, the train-induced settlement to the metro tunnel buried in the soft deposits is a potential problem.

By comparing the measured and the calculated results, it is concluded that the numerical simulation based on soil-water coupled elastoplastic analysis is necessary and feasible to reveal the train-induced vibration from a metro tunnel in the soft ground. Overall, the response characteristics of accelerations from the numerical simulation are very similar to the measured calculation.Numerical calculation also reveals that the acceleration changes from the tunnel to the ground surface, the acceleration and displacement amplification zones in the ground and on the ground surface, the slight increase of acceleration from saturated ground to single-phase ground. Besides, the EPWP accumulation can also be predicted by the numerical scheme proposed here, which is indeed an improvement to the previous numerical calculation. Accordingly, soil-water coupled numerical simulation is a favorable supplement to the field measurement to further understand the train-induced response characteristics in the soft deposits. It is found that the calculated accelerations in the ground are a little smaller than the measured values; this may be likely related to the low vibration frequency of the input train vibration load and

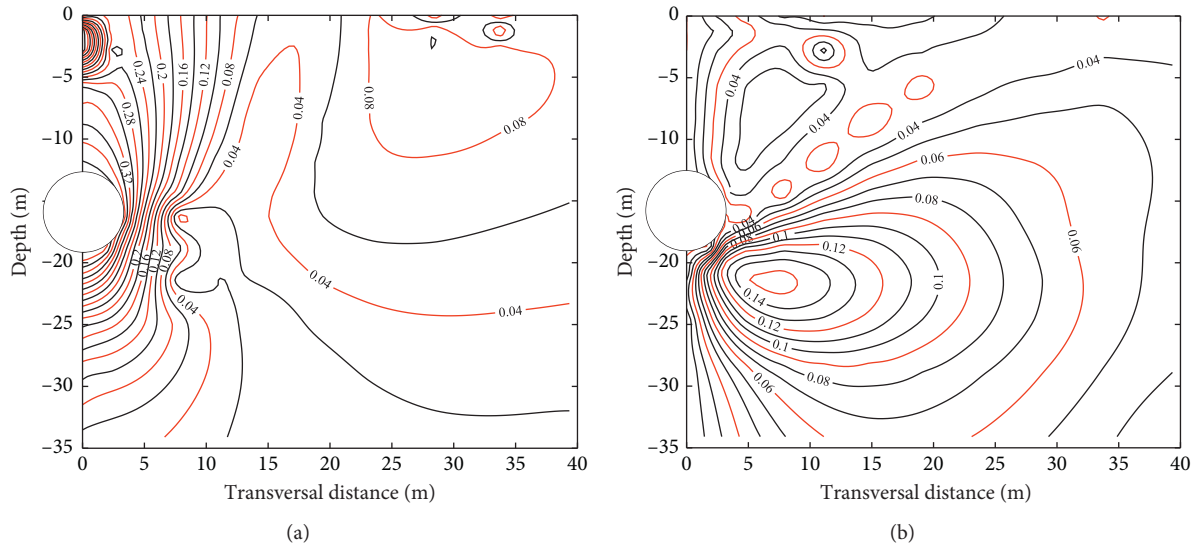

Figure 26: Displacement contour of the soft ground: (a) vertical direction; (b) transversal direction.

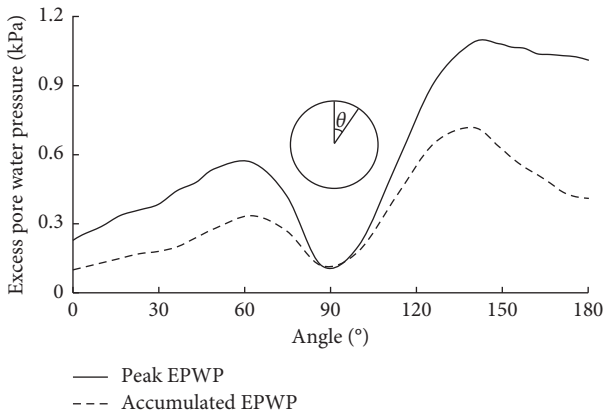

Figure 27: EPWP distribution around the tunnel.

the lack of consideration of the tunnel curvature. Since the dominant frequencies of the train vibration load determined from the analytical approach are generally less than 10 Hz [36], the underestimation of the ground vibrations are inevitable. The neglect of the tunnel curvature also weakens the ground vibration; however, our purpose in this study was primarily to make a full investigation on the response characteristics of the track-tunnel-ground system by combing the field measurement and numerical simulation. The acceleration discrepancy between numerical simulation and field measurement is not emphasized here, and further study can be conducted if better agreement between numerical and measurement results is required.

4. Conclusions

Field measurement and numerical simulation were conducted in this study to investigate the response characteristics from the tunnel interior to the ground surface. The peak acceleration, vibration level, and vibration frequency from the track, tunnel, and soft soil layers are analyzed to reveal the vibration propagation process. Based on the measured and calculated results, the following conclusions are obtained:

(1) The accelerations between the rail and the track bed or the tunnel wall belong to two different orders of magnitude. The acceleration is greatly attenuated from the rail to the track bed, but only slightly attenuated from the track bed to the tunnel wall. For the curved tunnel, the transversal vibration in the tunnel is also significant.

(2) Vertical ground vibration is dominant in the soft deposits. The maximum vertical acceleration locates at the bottom of the tunnel and attenuates like an arc in the transversal direction. There are transversal acceleration amplification phenomena in the ground, at a distance from the upper and the lower haunches of the tunnel. The train-vibration-affected region for the soft deposits is mainly within the range of 30 m away from the tunnel.

(3) The vibration frequency of the rail is broad and the dominant frequency mainly concentrates in the middle and high frequencies. The vibration frequency of the track bed and the tunnel wall drops to below 400 Hz while the frequency of the soft deposits drops to 200 Hz with two peak frequencies at 31.5 Hz and 125 Hz. The vibration dominant frequency on the ground surface is 20–100 Hz.

(4) Numerical simulation based on soil-water coupled elastoplastic analysis is effective to reveal the vibration attenuation characteristics from the tunnel interior to the ground surface; it also reveals the amplification zones of acceleration and displacement. The calculated results indicate that there is excess pore water pressure accumulation during each train vibration, which may lead to train-induced settlement in the metro tunnel in the long term.

Data Availability

The data used to support the findings of this study are available from the first author upon request.

Conflicts of Interest

The authors declare that they have no conflicts of interest.

Acknowledgments

The authors greatly appreciate the financial supports of the Natural Science Foundation of China (Grant no. 52008214), the Open Fund of Key Laboratory of Geotechnical and Underground Engineering of the Ministry of Education, Tongji University (Grant No. KLE-TJGE-B1904), and the Natural Science Foundation of Ningbo city (Grant no. 2019A610399).

References

[1] Y. B. Yang and L. C. Hsu, "A review of researches on ground-borne vibrations due to moving trains via underground tunnels," *Advances in Structural Engineering*, vol. 9, no. 3, pp. 377–392, 2006.

[2] X. Z. Sheng, "A review on modelling ground vibrations generated by underground trains," *International Journal of Rail Transportation*, vol. 7, no. 5, pp. 1–21, 2019.

[3] D. Clouteau, M. Arnst, T. M. Al-Hussaini, and G. Degrande, "Freefield vibrations due to dynamic loading on a tunnel embedded in a stratified medium," *Journal of Sound and Vibration*, vol. 283, no. 1-2, pp. 173–199, 2005.

[4] C. W. W. Ng, G. B. Liu, and Q. Li, "Investigation of the long-term tunnel settlement mechanisms of the first metro line in Shanghai," *Canadian Geotechnical Journal*, vol. 50, no. 6, pp. 674–684, 2013.

[5] S.-L. Shen, H.-N. Wu, Y.-J. Cui, and Z.-Y. Yin, "Long-term settlement behaviour of metro tunnels in the soft deposits of Shanghai," *Tunnelling and Underground Space Technology*, vol. 40, pp. 309–323, 2014.

[6] A. V. Metrikine and A. C. W. M. Vrouwenvelder, "Surface ground vibration due to a moving train in a tunnel: two-dimensional model," *Journal of Sound and Vibration*, vol. 234, no. 1, pp. 43–66, 2000.

[7] J. A. Forrest and H. E. M. Hunt, "A three-dimensional tunnel model for calculation of train-induced ground vibration," *Journal of Sound and Vibration*, vol. 294, no. 4-5, pp. 678–705, 2006.

[8] Z. Yuan, Y. Cai, and Z. Cao, "An analytical model for vibration prediction of a tunnel embedded in a saturated full-space to a harmonic point load," *Soil Dynamics and Earthquake Engineering*, vol. 86, pp. 25–40, 2016.

[9] S. Zhou, X. Zhang, H. Di, and C. He, "Metro train-track-tunnel-soil vertical dynamic interactions - semi-analytical approach," *Vehicle System Dynamics*, vol. 56, no. 12, p. 1945, 2018.

[10] S. Gupta, G. Degrande, and G. Lombaert, "Experimental validation of a numerical model for subway induced vibrations," *Journal of Sound and Vibration*, vol. 321, no. 3–5, pp. 786–912, 2009.

[11] X. Bian, H. Jiang, C. Chang, J. Hu, and Y. Chen, "Track and ground vibrations generated by high-speed train running on ballastless railway with excitation of vertical track irregularities," *Soil Dynamics and Earthquake Engineering*, vol. 76, pp. 29–43, 2015.

[12] M. Ma, W. Liu, C. Qian, G. Deng, and Y. Li, "Study of the train-induced vibration impact on a historic Bell Tower above two spatially overlapping metro lines," *Soil Dynamics and Earthquake Engineering*, vol. 81, pp. 58–74, 2016.

[13] C. He, S. Zhou, P. Guo, H. Di, and J. Xiao, "Dynamic 2.5-D Green's function for a point load or a point fluid source in a layered poroelastic half-space," *Engineering Analysis with Boundary Elements*, vol. 77, pp. 123–137, 2017.

[14] C. He, S. Zhou, P. Guo, H. Di, and X. Zhang, "Modelling of ground vibration from tunnels in a poroelastic half-space using a 2.5-D FE-BE formulation," *Tunnelling and Underground Space Technology*, vol. 82, pp. 211–221, 2018.

[15] G. Degrande, M. Schevenels, P. Chatterjee et al., "Vibration due to a test train at variable speeds in a deep bored tunnel embedded in London clay," *Journal of Sound and Vibration*, vol. 293, no. 3–5, pp. 626–644, 2006.

[16] D. P. Connolly, P. A. Costa, G. Kouroussis, P. Galvin, P. K. Woodward, and O. Laghrouche, "Large scale international testing of railway ground vibrations across Europe," *Soil Dynamics and Earthquake Engineering*, vol. 77, pp. 1–12, 2006.

[17] S. Gupta, W. F. Liu, G. Degrande, G. Lombaert, and W. N. Liu, "Prediction of vibrations induced by underground railway traffic in Beijing," *Journal of Sound and Vibration*, vol. 310, no. 3, pp. 608–630, 2008.

[18] M. L. Lou, X. P. Jia, and J. Q. Yu, "Field measurement and analysis of ground vibration induced by train induced by subway trains," *Journal of Disaster Prevention and Mitigation Engineering*, vol. 29, no. 3, pp. 282–288, 2009, in Chinese.

[19] P. H. Liu, Y. Q. Yang, and J. Ying, "Test and analysis on vibration of different track structures in tunnel," *Journal of Vibration and Shock*, vol. 33, no. 2, pp. 31–37, 2014, in Chinese.

[20] C. Zou, Y. Wang, P. Wang, and J. Guo, "Measurement of ground and nearby building vibration and noise induced by trains in a metro depot," *Science of the Total Environment*, vol. 536, pp. 761–773, 2015.

[21] Z. Cao, T. Guo, Z. Zhang, and A. Li, "Measurement and analysis of vibrations in a residential building constructed on an elevated metro depot," *Measurement*, vol. 125, pp. 394–405, 2018.

[22] Q. Jin, D. J. Thompson, D. E. J. Lurcock, M. G. R. Toward, and E. Ntotsios, "A 2.5D finite element and boundary element model for the ground vibration from trains in tunnels and validation using measurement data," *Journal of Sound and Vibration*, vol. 422, pp. 373–389, 2018.

[23] T. Y. Wang, "Study on subway-induced environmental vibration and isolation method of building of it," Dissertation in Chinese, Tongji University, Shanghai, China, 2008.

[24] W. F. Liu, "Study on numerical prediction model of metro train induced vibrations in tunnels and free field," Dissertation in Chinese, Beijing Jiaotong University, Beijing, China, 2009.

[25] B. Ye, G. Ye, F. Zhang, and A. Yashima, "Experiment and numerical simulation of repeated liquefaction-consolidation of sand," *Soils and Foundations*, vol. 47, no. 3, pp. 547–558, 2007.

[26] Q. Huang, H.-w. Huang, B. Ye, D.-m. Zhang, L.-l. Gu, and F. Zhang, "Dynamic response and long-term settlement of a metro tunnel in saturated clay due to moving train load," *Soils and Foundations*, vol. 57, no. 6, pp. 1059–1075, 2017.

[27] J. Lysmer and R. Kuhlemeyer, "Finite dynamic model for infinite media," *Journal of Engineering Mechanics*, vol. 95, no. 4, pp. 859–878, 1969.

[28] F. Zhang, B. Ye, T. Noda, M. Nakano, and K. Nakai, "Explanation of cyclic mobility of soils: approach by stress-induced anisotropy," *Soils and Foundations*, vol. 47, no. 4, pp. 635–648, 2007.

[29] K. Hashiguchi and M. Uendo, "Elastoplastic constitutive laws of granular material, constitutive equations of soils," in *Proceedings of the 9th International Conference on Soil Mechanics and Foundation Engineering*, pp. 73–82, Tokyo, Japan, July 1977.

[30] A. Asaoka, M. Nakano, and T. Noda, "Superloading yield surface concept for highly structured soil behavior," *Soils and Foundations*, vol. 40, no. 2, p. 99, 2000.

[31] Z.-F. Xia, G.-L. Ye, J.-H. Wang, B. Ye, and F. Zhang, "Fully coupled numerical analysis of repeated shake-consolidation process of earth embankment on liquefiable foundation," *Soil Dynamics and Earthquake Engineering*, vol. 30, no. 11, pp. 1309–1318, 2010.

[32] L.-l. Gu, G.-l. Ye, X.-h. Bao, and F. Zhang, "Mechanical behaviour of piled-raft foundations subjected to high-speed train loading," *Soils and Foundations*, vol. 56, no. 6, pp. 1035–1054, 2016.

[33] X. Bao, Z. Xia, G. Ye, Y. Fu, and D. Su, "Numerical analysis on the seismic behavior of a large metro subway tunnel in liquefiable ground," *Tunnelling and Underground Space Technology*, vol. 66, pp. 91–106, 2017.

[34] G.-l. Ye and B. Ye, "Investigation of the overconsolidation and structural behavior of Shanghai clays by element testing and constitutive modeling," *Underground Space*, vol. 1, no. 1, pp. 62–77, 2016.

[35] Y.-Q. Tang, Z.-D. Cui, X. Zhang, and S.-K. Zhao, "Dynamic response and pore pressure model of the saturated soft clay around the tunnel under vibration loading of Shanghai subway," *Engineering Geology*, vol. 98, no. 3-4, pp. 126–132, 2008.

[36] H. Xia, Y. M. Cao, and N. Zhang, "Numerical analysis of vibration effects of metro trains on surrounding environment," *International Journal of Structural Stability and Dynamics*, vol. 7, no. 1, pp. 151–166, 2007.